High-density transposon mutagenesis in *Mycobacterium abscessus* identifies an essential penicillin-binding lipo-protein (PBP-lipo) involved in septal peptidoglycan synthesis and antibiotic sensitivity

Chidiebere Akusobi[1], Bouchra S. Benghomari[2], Ian D. Wolf[1], Shreya Singhvi[3], Junhao Zhu[1], Thomas R. Ioerger[4], Eric J. Rubin[1]

[1]Department of Immunology and Infectious Diseases, Harvard T.H. Chan School of Public Health, Boston, MA 02115, USA

[2]Department of Biology, Northeastern University, Boston, MA 02115, USA

[3]Department of Molecular and Cell Biology, University of California, Berkeley, Berkeley, CA 94720, USA

[4]Department of Computer Science and Engineering, Texas A&M University, College Station Texas 77843, USA

Abstract

Mycobacterium abscessus (*Mab*) is a rapidly growing non-tuberculous mycobacterium (NTM) that causes a wide range of infections. Treatment of *Mab* infections is difficult because the bacterium is intrinsically resistant to many classes of antibiotics. Developing new and effective treatments against *Mab* requires a better understanding of the unique vulnerabilities that can be targeted for future drug development. To achieve this, we identified essential genes in *Mab* by conducting transposon-sequencing (TnSeq) on the reference *Mab* strain ATCC 19977. We generated ~51,000 unique transposon mutants and used this high-density library to identify 362 essential genes for *in vitro* growth. To investigate species-specific vulnerabilities in *Mab*, we further characterized *MAB_3167c*, a predicted penicillin-binding-lipoprotein (PBP-lipo) that is essential in *Mab* and non-essential in *M. tuberculosis* (*Mtb*). We found that PBP-lipo primarily localizes to the subpolar region and later to the septum as cells prepare to divide. Knockdown of *Mab* PBP-lipo causes cells to elongate, develop ectopic branches, and form multiple septa. Dual knockdown of PBP-lipo with PBPs, PbpB, DacB1, and a carboxypeptidase, MAB_0519 lead to synergistic growth arrest. In contrast, these genetic interactions were absent in the *Mtb* model organism, *M. smegmatis*, indicating that the PBP-lipo homologs in the two species exist in distinct genetic networks. Finally, repressing PBP-lipo sensitized the reference strain and 11 *Mab* clinical isolates to several classes of antibiotics, including the β-lactams, ampicillin and amoxicillin by greater than 128-fold. Altogether, this study presents PBP-lipo as a key enzyme to study *Mab* specific processes in cell wall synthesis and importantly positions PBP-lipo as an attractive drug target to treat *Mab* infections.

Introduction

Mycobacterium abscessus (*Mab*) is the most common cause of human disease among the rapidly growing non-tuberculous mycobacteria (NTM). It causes a wide range of illnesses including lung, skin and soft-tissue infections, as well as disseminated disease (1–3). While the incidence of *Mab* infections is rising worldwide, treating *Mab* infections remains difficult. The bacterium has intrinsic and acquired resistance mechanisms to many classes of antibiotics, including the standard drugs used to treat tuberculosis (4,5). The current treatment regimen for *Mab* requires taking a combination of multiple antibiotics for up to 18 months and is often associated with severe toxicity and routinely ends in treatment failure (6). Thus, there is an urgent need for new and effective drugs to treat the emerging global public health threat of *Mab* infections (7).

Developing novel antibiotic treatments for *Mab* requires a better understanding of essential biological processes in the bacterium that can be targeted. Identifying essential genes is the first step in this process, and by combining transposon-mutagenesis with massive parallel sequencing, transposon-sequencing (TnSeq) has been an effective tool to determine gene essentiality on a genome-wide scale in other microbes (8). However, while many TnSeq screens have been conducted in *M. tuberculosis* (*Mtb*) (9), up until recently only 2 published TnSeq screens have been reported in *Mab* (10,11). While both *Mab* TnSeq screens have provided tools and important insights into *Mab* biology, neither utilized a mutant library with high enough density to comprehensively identify essential genes. This changed with the recent publication from Rifat *et al*, who generated robust high-density transposon libraries of *Mab* and identified a comprehensive list of genetic elements essential for *in vitro* growth (12). Identification of these essential genes serves as an excellent starting point to classify attractive targets for drug discovery.

67 One major target of antibiotics is the mycobacterial cell wall whose biogenesis is essential for
68 bacterial growth (13,14). The structure of the mycobacterial cell wall is unique among bacteria
69 because it is composed of three macromolecules: peptidoglycan (PG), arabinogalactan, and
70 mycolic acids. Together, these layers envelop mycobacteria with a thick, waxy coat that forms a
71 permeability barrier to many drugs (15,16). The foundational layer is comprised of peptidoglycan
72 (PG), which consists of glycan sugars cross-linked by short peptides forming a continuous, net-
73 like structure that maintains cell shape and prevents rupture. Mycobacteria build new PG at the
74 cell poles aided by Class A penicillin binding proteins (PBPs) that perform two reactions: a
75 transglycosylation reaction that polymerizes PG monomers to existing glycan strands and a
76 transpeptidation reaction that cross-links glycan strands to each other (17). Class B PBPs solely
77 perform the cross-linking reactions (18,19). A hallmark of PBPs is that they are inhibited by β-
78 lactam antibiotics; however, these antibiotics are typically not used to treat *Mab* infections due
79 to high levels of resistance and the presence of β-lactamases in the genome (20).
80
81 To identify essential genes for *in vitro* growth and classify potential new drug targets in *Mab*, we
82 performed TnSeq. We generated high-density transposon libraries of ~51,000 mutants in the
83 reference strain, *M. abscessus subsp. abscessus* ATCC 19977 and identified 362 genes
84 required for *in vitro* growth. We next identified essential genes in *Mab* that were non-essential in
85 *Mtb* in order to study species-specific vulnerabilities in *Mab*. From this list of genes, we further
86 characterized *MAB_3167c*, which encodes PBP-lipo, a conserved Class B PBP. We found that
87 PBP-lipo is required for normal peptidoglycan (PG) synthesis, cell division, and sensitizes *Mab*
88 to commonly-used β-lactams and other classes of antibiotics. None of these phenotypes were
89 present in the *Msm* and *Mtb* PBP-lipo knockouts. Thus, we find that PBP-lipo has a unique
90 essential function in *Mab* and is a potential drug target for treating *Mab* infections.

Results

Identification of *M. abscessus* ATCC 19977 essential genes for *in vitro* growth

To identify essential genes in *Mab*, we performed TnSeq on *M. abscessus subsp. abscessus* ATCC 19977 (hereafter referred to as *Mab*) using the ϕMycoMar T7 phage carrying the Himar1 transposon for transduction. This transposon inserts into 'TA' dinucleotide sites and disrupts gene function (Figure 1A) (21). We transduced three independently grown cultures of *Mab*, yielding triplicate libraries with saturations of 54.2%, 62.3%, and 64.1% for Library 1, 2, and 3 respectively (Supplemental Table 1). The average Pearson r^2 correlation of mean read counts for each gene across 2 libraries was 0.85 indicating good correlation among the libraries (Supplemental Figure 1). The transposon insertions across the three libraries were mapped onto the *Mab* genome as depicted in the chromosome map (Figure 1B). Across three libraries, we generated approximately 51,000 unique transposon mutants, as defined by sites of unique transposon insertions across all three libraries. Of note, the *Mab* libraries shared the same non-permissive 'TA' sites for transposon insertion as has been described in other mycobacterial species (Shoudhery *et al*, bioRxiv 2021).

The high density of these libraries allowed us to identify essential *Mab* genes using the Hidden Markov Model (HMM) algorithm implemented by TRANSIT (22). HMM identified 362 genes as essential, 4167 as non-essential, 153 as producing growth defect when disrupted, and 233 as causing a growth advantage when disrupted (Figure 1C, Supplemental Table 2). As expected, many of the genes identified as essential were involved in key biological processes including protein translation, amino acid metabolism, and cell wall biogenesis based on Clusters of Orthologous Groups (COG) analysis (Figure 1E).

Identification and Validation of uniquely essential genes in *Mab*

117 Understanding differences in essential genes between *Mab* and *Mtb* might uncover new ways of
118 specifically targeting *Mab*. Thus, we identified *Mab*-specific essential genes by comparing gene
119 essentiality between mutual orthologs of *Mab* and *Mtb.* We used *Mtb* essentiality data
120 generated from a comprehensive analysis on *Mtb* essentiality using 14 high-quality TnSeq
121 datasets (9). Of the 2279 mutual orthologs between *Mab* and *Mtb*, 282 genes were essential in
122 both species. We focused on the mutual orthologs that that were essential in *Mab,* but non-
123 essential in *Mtb*. These genes could potentially represent *Mab* specific drug targets. Exactly 20
124 genes fit into this category, which we refer to as "uniquely essential" (Figure 1D) (Supplemental
125 Table 3).
126
127 To understand the quality of predictions by TnSeq, we validated the essentiality of a subset of
128 genes using an anhydrotetracycline (ATc) inducible CRISPRi system developed for use in *Mtb*
129 (23). Expression of a non-targeting sgRNA control in this system has no impact on cell
130 proliferation (Figure 2A). In contrast, repressing canonical essential genes *rpoB, gyrB,* and *secY*
131 impaired cell growth in both liquid broth (Figure 2A) and solid media (Supplemental Figure 2A),
132 indicating that the CRISPRi system developed in *Mtb* functions in *Mab*.
133
134 We next validated the essentiality of a subset of the 20 uniquely essential genes in *Mab*: *glnA2,*
135 *icd2, sdhA,* and *MAB_4471*. CRISPRi knockdown of these uniquely essential genes impaired
136 growth in liquid media (Figure 2B) as well as solid media (Supplemental Figure 2B). These
137 results confirm that at least a subset of uniquely essential *Mab* genes identified by TnSeq are
138 required for optimal *in vitro* growth. The slight rise in OD_{600} later in the time course is consistent
139 with the emergence of escape mutants in the CRISPRi system, which has been previously
140 described (24,25).
141
142 **PBP-lipo is uniquely essential in *Mab***

143 One of the uniquely essential genes we identified was *MAB_3167c*, which encodes a Class B
144 penicillin-binding lipoprotein (PBP-lipo). PBP-lipo is predicted to have a single N-terminal
145 transmembrane helix and a transpeptidase domain. From our *Mab* TnSeq data, *MAB_3167c*
146 lacked transposon insertions across all three replicate libraries (Figure 3A). This finding
147 corroborates data from previously generated *Mab* transposon libraries that show lack of
148 insertions in *MAB_3167c* (10,12). Comparing the essentiality of PBP enzymes in *Mab* with their
149 homologs in *Mtb* revealed that *pbp-lipo* is unique in being the sole PBP whose essentiality
150 differs between the two species. Specifically, *pbp-lipo* is essential in *Mab* and non-essential in
151 *Mtb in vitro* (Figure 3B).
152
153 To validate that PBP-lipo is required for *in vitro* growth, we used the CRISPRi system to induce
154 knockdown using constructs encoding 1, 2, or 3 sgRNAs targeting *pbp-lipo* (Supplemental
155 Figure 3A). The single, double, or triple sgRNA constructs allowed for the fine tuning of the
156 magnitude of *pbp-lipo* knockdown, as measured by RT-qPCR (Supplemental Figure 3B). We
157 noted that the empty vector control (0 sgRNA) and single sgRNA construct had no detectable
158 effect on the growth of *Mab* (Supplemental Figure 3C). In contrast, when *pbp-lipo* was targeted
159 with either 2 or 3 sgRNAs, the growth of *Mab* was inhibited, indicating that *pbp-lipo* is indeed
160 required for optimal *in vitro* growth (Figure 3C). We also observed the inhibition of cell growth on
161 solid media where knockdown of PBP-lipo by 2 sgRNA and 3 sgRNA vectors led to a 1000-fold
162 reduction in colony forming units (CFU) (Supplemental Figure 3D). To complement the PBP-lipo
163 knockdown growth defect phenotype, we recoded a version of PBP-lipo with the protospacer
164 adjacent motif (PAM) sequence mutated. This prevents sgRNAs from binding the introduced
165 PBP-lipo copy present on the integrated plasmid. When constitutively expressed, this recoded
166 PBP-lipo rescued growth of the native PBP-lipo knockdown (Supplemental Figure 3D). In
167 contrast, a recoded and catalytically-dead mutant of PBP-lipo did not rescue growth. This data
168 demonstrates that PBP-lipo's transpeptidase activity is required for *Mab* optimal growth.

169

170 In contrast to *Mab*, when we deleted the gene encoding PBP-lipo in *Mtb*, *Rv2864c*, the growth
171 of the knockout and wild-type strains was indistinguishable (Figure 3D). Similarly, the PBP-lipo
172 homolog in *Msm, MSMEG_2584c*, when knocked out grew identically to wildtype with no growth
173 defect (Supplemental Figure 4). Taken together, these data demonstrate that PBP-lipo is
174 essential for growth in *Mab,* while its homologs in *Mtb* and *Msm* are non-essential.

175

176 **PBP-lipo is required to maintain normal cell elongation and division**

177 A hallmark of PBPs is that they bind β-lactam antibiotics. Therefore, to test whether PBP-lipo is
178 an active PBP in *Mab*, we determined whether PBP-lipo binds bocillin FL, a fluorescent analog
179 of penicillin (26). Using a strain that constitutively expresses a strep-tagged PBP-lipo, we
180 identified a fluorescent bocillin FL band at the same molecular weight as PBP-lipo, which was
181 confirmed to be PBP-lipo by Western blot (Supplemental Figure 5). These data suggest that
182 PBP-lipo binds bocillin FL *in vivo* and is an active PBP. Interestingly, in wildtype *Mab,* we did not
183 detect an obvious PBP-lipo band at the predicted molecular weight of PBP-lipo, 63 kDa,
184 suggesting that native expression levels of PBP-lipo is either low or PBP-lipo is expressed at
185 distinct times during the cell cycle.

186

187 In mycobacteria, the PG layer is critical for maintaining normal cell shape and altering PBP
188 expression often results in abnormal cell morphology. Thus, we studied the morphology of *Mab*
189 when PBP-lipo was repressed and discovered dramatic morphological changes. *Mab* cells
190 elongate, branch inappropriately, and form ectopic poles of active growth, as evidenced by
191 staining with NADA, a fluorescent-D-amino acid (FDAA) that binds areas of active PG synthesis
192 (27) (Figure 4A). PBP-lipo knockdown significantly increased the number of cells with ectopic
193 branches (Supplemental Figure 6B). Furthermore, during normal growth of *Mab*, a small
194 percentage of cells contain one mid-cell FDAA band, indicating active PG synthesis at the site

195 of septation. However, when PBP-lipo is knocked down, we occasionally find cells with 2 or 3
196 bands mid-cell, as exemplified in the 2 sgRNA + panel (Figure 4A). PBP-lipo knockdown strains
197 were all significantly longer than their uninduced controls, with the longest average cell length
198 belonging to the strain with the strongest PBP-lipo knockdown (Figure 4B). Of note, while the 0
199 sgRNA +/- cells are by eye morphologically indistinguishable, there is a statistically significant
200 difference in the mean cell lengths, likely due to the effect of ATc on cells (Figure 4B). Notably,
201 cell width did not change among the strains (Supplemental Figure 6A). In comparison, in *Msm*
202 and *Mtb*, there were no differences in morphology and cell length between the wildtype and
203 PBP-lipo knockout strains (Supplemental Figure 7). The dramatic changes in *Mab* morphology
204 when PBP-lipo is repressed suggests proper expression of this enzyme is required for
205 maintaining normal *Mab* elongation and division.
206
207 **PBP-lipo localizes to the subpolar regions and to the mid-cell before cell division**
208 The morphological defects caused by PBP-lipo knockdown were reminiscent of septal factor
209 depletions observed in *Msm* (28). Thus, we hypothesized that PBP-lipo localizes to the septum.
210 To test this hypothesis, we N-terminally tagged PBP-lipo with mRFP, which has been previously
211 shown to function in the mycobacterial periplasm (29). This mRFP-PBP-lipo construct was
212 constitutively expressed and visualized with fluorescence microscopy. We discovered that PBP-
213 lipo localized to the subpolar regions of the cell and the mid-cell, likely in the growing septum
214 (Figure 5A)**.** The resulting microscopy images were analyzed using OMEGA, which quantified
215 the fluorescent signal across the cell normalized by cell length (Zhu *et al*, unpublished). We then
216 binned the cells into quartiles according to their length and found that the mRFP-PBP-lipo
217 fluorescent signal was concentrated at the sub-polar regions for cells of all lengths, while the
218 mid-cell localization of PBP-lipo was only present in the longest cells in the population (Figure
219 5B). These data suggest that as cells elongate, PBP-lipo localizes to the septum and is likely
220 involved in septum formation and cell division.

221

222 **PBP-lipo is incorporated into a unique PG network in *Mab* that does not exist in *Msm***

223 Given that *Mtb* and *Msm* do not have duplicates of PBP-lipo in their genomes, we hypothesized
224 other reasons for the differential essentiality of PBP-lipo between these species. It is possible
225 that there is a functional difference between PBP-lipo in *Mab* and its homologs in *Msm* and *Mtb*.
226 This possibility intrigued us because an alignment of PBP-lipo from various mycobacteria
227 revealed that PBP-lipo$_{Mab}$ has 5 additional amino acids present only in the *Mab* homolog
228 (Supplemental Figure 8A). When *in silico* structures of PBP-lipo$_{Mab}$ and PBP-lipo$_{Mtb}$ are
229 modeled, these 5 extra residues form an appendage we hypothesized could impart PBP-lipo$_{Mab}$
230 with additional ability to bind proteins (Supplemental Figure 8B).

231

232 To test this hypothesis, we constitutively expressed PBP-lipo$_{Msm}$ in the 2 sgRNA *Mab* strain
233 (hereafter referred to as the *Msm* complement strain). As expected, knockdown of the native
234 *Mab* PBP-lipo impairs growth. However, PBP-lipo$_{Msm}$ expression in the 2 sgRNA strain rescued
235 *Mab* growth (Figure 6A). Furthermore, expressing PBP-lipo$_{Msm}$ eliminated the branching
236 phenotype of the native PBP-lipo knockdown and partially reversed the elongated phenotype as
237 well (Figure 6B). The recoded version of PBP-lipo$_{Mab}$ also reversed the branching of cells and
238 partially complemented the elongated phenotype (Figure 6B). In contrast, the catalytically-dead
239 version of PBP-lipo$_{Mab}$-(S364A) did not complement, with cells appearing elongated and
240 branched (Figure 6B, Supplemental Figure 9). These results demonstrate that PBP-lipo$_{Msm}$ can
241 rescue knockdown of the endogenous *Mab* enzyme. From these data, we conclude that the
242 essentiality of PBP-lipo$_{Mab}$ is not solely due to a unique functional property that is present only in
243 the *Mab* homolog.

244

245 An alternative hypothesis is PBP-lipo participates in a PBP interaction network in *Mab* that is
246 distinct from respective PBP networks in *Msm* and *Mtb*. In short, while PBP-lipo is required in

247 the *Mab* PBP network*,* its function is likely redundant in the networks of *Msm* and *Mtb.* This
248 notion of functionally distinct PBP networks has been previously described in mycobacteria (30).
249 To interrogate the PBP network of *Mab*, we tested which PBPs genetically interacted with PBP-
250 lipo. To perform this experiment, we cloned CRISPRi constructs with sgRNAs that would weakly
251 knockdown each PBP in *Mab* (PBPx) so that growth was not significantly impaired. We also
252 cloned combinatorial CRISPRi constructs where PBP-lipo and another PBP were weakly
253 repressed. Using this dual sgRNA vector, we could simultaneously knockdown PBP-lipo and a
254 PBP of interest.
255
256 Using combinatorial knockdowns of each PBP, we compared growth inhibition when a single
257 PBP was knocked down versus when PBP-lipo and a second PBP were jointly repressed. Of
258 the 8 combinations we tested, we found that knockdown of three PBPs with PBP-lipo lead to
259 synergistic growth arrest (Figure 6C). These enzymes were *pbpB, dacB1,* and *MAB_0519,*
260 which encodes a protein with a hypothesized carboxypeptidase domain. This genetic synergy
261 was also observed in liquid culture for *pbpB* and *dacB1* (Supplemental Figure 10A). The
262 homolog of PbpB is a well-studied enzyme in both *Msm, Mtb,* and the model organisms *E. coli*
263 and *B. subtilis,* where it is known as FtsI*.* In all these organisms, PbpB localizes to the septum
264 and is largely responsible for septal PG synthesis (31–33). Interestingly, like PbpB and PBP-
265 lipo, we found DacB1 localizes to the septum (Supplemental Figure 10B). These data suggest
266 that PBP-lipo genetically interacts with PbpB and DacB1, and that all three enzymes localize to
267 the same region of the cell and could potentially coordinate septal PG synthesis in a complex
268 together.
269
270 We next tested whether the same PBP-lipo genetic interactions existed in *Msm.* We used
271 CRISPRi to knockdown *Msm* PBP homologs in the wildtype *Msm* and the *pbp-lipo* knockout
272 background. In this experiment, genes that interacted with PBP-lipo would show impaired cell

273 growth when repressed in the PBP-lipo knockout. Interestingly, we did not observe genetic
274 interactions between any of the PBPs tested and PBP-lipo (Figure 6D). This was true for the
275 PBPs tested with homologs in *Mab* and additional PBPs present in the *Msm* genome
276 (Supplemental Figure 11).
277
278 We next used a whole genome approach to identify genes in *Msm* that genetically interact with
279 PBP-lipo. We generated high density transposon mutant libraries in both the wildtype and PBP-
280 lipo knockout strains of *Msm* to identify genes that were conditionally essential in the knockout
281 background. The saturation of the 2 wildtype libraries were 51.9% and 53.4%, while the
282 saturation of the PBP-lipo knockout library was 62.4%. Using the resampling method in
283 TRANSIT, our TnSeq data revealed that there were no conditionally essential genes in the
284 ΔPBP-lipo *Msm* background (Supplemental Table 4). These data strongly suggest PBP-lipo in
285 *Msm* exists in a robust genetic network with multiple functional redundancies. To uncover PBP-
286 lipo's function in *Msm*, it is possible that double and triple knockout mutants of PG synthesis
287 enzymes would need to be generated.
288
289 **Repressing PBP-lipo sensitizes *Mab* to a wide range of antibiotics**
290 Given PBP-lipo's essentiality in *Mab* and the genetic interactions it has with other PBPs, we
291 hypothesized that repressing PBP-lipo would affect *Mab*'s sensitivity to antibiotics, including β-
292 lactams. To test this hypothesis, we measured the sensitivity of PBP-lipo knockdown cells to 21
293 antibiotics that target translation, transcription, and DNA replication in both *Mab* and *Msm*.
294
295 Wildtype *Mab* is typically resistant to β-lactams amoxicillin and ampicillin with MICs greater than
296 >256 µg/ml. When PBP-lipo is knocked down, the MIC for both antibiotics dropped to 2 µg/ml,
297 indicating a greater than 128-fold sensitization (Table 1). These results indicate a strong

298 chemical-genetic interaction between PBP-lipo and both ampicillin and amoxicillin. Interestingly,
299 not all β-lactams had shifts in their MIC when PBP-lipo was knocked down. This indicates that
300 there is a specific chemical-genetic interaction between PBP-lipo and ampicillin and amoxicillin.
301 MIC changes for other β-lactams were less drastic, with a 4-8- fold reduction observed for
302 faropenem and cefoxitin (Table 1). PBP-lipo knockdown also affects susceptibility to antibiotics
303 that do not target the cell wall. The macrolides, clarithromycin and erythromycin, were 128-fold
304 and 64-fold more potent respectively in the PBP-lipo knock down cells. A 16-fold reduction in
305 MIC was observed for RNA polymerase inhibitor, rifampicin.
306
307 The MIC differences in rifampicin and clarithromycin are notable because these antibiotics do
308 not target the cell wall. Thus, the mechanism of synergy between PBP-lipo repression and these
309 antibiotics likely differs from the synergy with ampicillin and amoxicillin. We posited that PBP-
310 lipo repression might increase the permeability of the cell wall, allowing more drug to enter the
311 cell. To test this hypothesis, we measured the accumulation of calcein into *Mab*, which is proxy
312 for cell permeability. Calcein accumulates more rapidly in PBP-lipo knockdown cells, indicating
313 that PBP-lipo increases the permeability of *Mab* cells (Supplemental Figure 13). This increased
314 permeability likely leads to increased antibiotic access to the cell, thus sensitizing the bacteria to
315 the antibiotics.
316
317 When the MICs of the same 21 antibiotics tested in *Mab* were measured in the PBP-lipo
318 knockout in *Msm,* we observed no difference in the MICs (Supplemental Table 5). We also
319 measured the MICs of a subsection of these antibiotics in the *pbp-lipo* knockout in *Mtb* and
320 found no difference in MICs between the wildtype and knockout strain (Supplemental Table 6).
321 These data suggest that PBP-lipo's unique function in *Mab's* PG synthesis network likely
322 contributes to the bacterium's sensitivity to antibiotics when the enzyme is repressed.

323

324 **Repression of PBP-lipo sensitizes *Mab* clinical isolates to antibiotics**

325 The antibiotic experiments were conducted on the ATCC 19977 reference strain on *Mab*, which
326 is lab adapted, after being isolated from a knee abscess in the 1950s and propagated in the lab
327 since (3,34). Work performed in *Mtb* has demonstrated clinical isolates and lab-adapted strains
328 respond to antibiotics stressors differently (35). As a result, we tested whether knockdown of
329 PBP-lipo in *Mab* clinical isolates led to the same changes in antibiotic sensitivity as observed in
330 the reference strain.

331

332 We found that knockdown of PBP-lipo using the 3 sgRNA construct impaired cell growth in all
333 11 clinical isolates leading to a 100 to 10,000-fold difference in CFUs (Supplemental Figure
334 12A). We also confirmed in a sub-set of the clinical isolates that PBP-lipo knockdown lead to
335 elongated and inappropriately branched cells, as observed in the reference strain
336 (Supplemental Figure 12B). After confirming the PBP-lipo phenotypes in the clinical isolates, we
337 measured the MICs of ampicillin, amoxicillin, meropenem, rifampicin, and clarithromycin on *pbp-*
338 *lipo* knockdowns of the clinical isolates.

339

340 For amoxicillin and ampicillin, PBP-lipo knockdown reduced the MICs by >32 to >512-fold.
341 Meropenem served as a negative control and indeed, there was no difference in MICs between
342 uninduced and induced strains (Table 2). Finally, we observed an >8X-32X fold difference in the
343 MICs for rifampicin and 8 to 128-fold difference in the MICs for clarithromycin (Table 3).
344 Altogether, the antibiotic sensitivity data demonstrate that the phenotypic consequences of
345 repressing PBP-lipo is not only limited to the lab-adapted reference strain, but is also observed
346 in *Mab* clinical isolates.

347 **Discussion**

348 Developing new drugs and drug regimens against *Mab* requires a better understanding of the
349 bacterium's essential processes. This includes identifying essential *Mab* genes for further
350 characterization as potential drug targets. To do this, we generated high-density transposon
351 libraries to identify essential genes in the reference strain, *M. abscessus subsp. abscessus*
352 ATCC 19977*.* Importantly, *Mab* transposon libraries with fewer than 10,000 unique mutants
353 have been previously published, but these studies did not fully identify the list of essential genes
354 in *Mab* (10,11). Recently, Rifat *et al* successfully generated high-density libraries and were the
355 first group to identify essential genes and genomic elements in the *Mab* genome (12). All
356 together, they identified 326 essential genes and compared this list to essential genes identified
357 in *Mtb* and *Mycobacterium avium.* Similar to our study, Rifat *et al* highlighted uniquely essential
358 genes in *Mab,* which they also state deserve further study as these genes could represent *Mab*
359 specific drug targets (12).

360

361 In addition to identifying essential genes in *Mab*, our study builds off of Rifat *et al's* work by
362 using CRISPRi to efficiently repress gene expression and validate predicted essential genes as
363 required for *in vitro* growth (23). Furthermore, we found that by targeting genes with multiple
364 sgRNAs, CRISPRi can achieve significant gene repression, allowing for the investigation of
365 essential genes and providing an alternative to gene knockouts. Constructing gene knockouts in
366 *Mab* can be inefficient (36); thus, CRISPRi provides a convenient tool for genetic manipulation
367 in *Mab.* Overall, the newly generated *Mab* transposon libraries can be used to determine genes
368 required for growth in a variety of conditions including infection models, biofilms, and antibiotic
369 stress.

370

371 Both Rifat *et al's* and our TnSeq data identified PBP-lipo as the sole peptidoglycan synthesis
372 gene that was essential in *Mab* and non-essential in *Mtb* (12)*.* Using CRISPRi, we

373 demonstrated the necessity of PBP-lipo expression for *Mab* to maintain normal morphology and
374 to divide properly. When PBP-lipo is repressed, cells elongate, branch, and form ectopic poles.
375 We localized PBP-lipo to the subpolar regions of the cell, and as cells elongate and prepare for
376 division, PBP-lipo localizes to the septum. This constellation of phenotypes mimic septal-factor
377 depletions observed in *Msm,* which also causes cells to elongate, branch, and form ectopic
378 poles (28). These data suggest that PBP-lipo is involved with PG synthesis at the septum and
379 that depletion of the enzyme likely leads to dysregulated septal PG synthesis and aberrant cell
380 division.
381
382 Given PBP-lipo's localization and effect on cell division, we posit PBP-lipo acts as an essential
383 septal PG synthesis enzyme in *Mab.* In *Mtb* and *Msm,* this is accomplished by the enzyme
384 *pbpB*, which is essential for growth. Additionally, when *pbpB* is repressed in these species, cells
385 appear morphologically similar to the PBP-lipo knockdown in *Mab* (28,31). Interestingly, PBP-
386 lipo knockouts in both *Msm* and *Mtb* are morphologically identical to wildtype cells
387 (Supplemental Figure 7). These data underscore the notion that biological insights from *Msm*
388 and *Mtb* should not be de-facto applied to *Mab*. We hypothesize that PBP-lipo is a member of
389 the *Mab* divisome complex, a collection of structural proteins and enzymes that coordinates cell
390 division (37). Future studies are needed to determine if PBP-lipo interacts with known septal
391 factors, such as FtsQ, FtsW, FtsZ, whose functions have been described in *Msm* (38–40).
392 Future work may also reveal novel PBP-lipo binding factors that coordinate PG synthesis and
393 cell division in *Mab*.
394
395 Phenotypes characteristic of the PBP-lipo knockdown in *Mab* were absent in the *Mtb* and *Msm*
396 PBP-lipo knockouts. Both *Mtb* and *Msm* do not have a duplicate copy of PBP-lipo in their
397 genomes. Thus, to explain the differential essentiality of PBP-lipo across these mycobacterial
398 species, one hypothesis we explored was differences in the genetic networks of PG synthesis

399 enzymes. Construction of the PG layer is a complex process that involves a collection of
400 enzymes that work in concert to ensure proper synthesis and remodeling. Previous work has
401 shown that PG synthesis enzymes belong to genetic and spatiotemporal networks that do not
402 necessarily replicate across closely related species (30,41). Thus, while the building blocks to
403 construct the PG layer may be similar between species, how the enzymes are networked and
404 subsequently function together may differ. We demonstrated that PBP-lipo genetically interacts
405 with *pbpB, dacB1,* and *MAB_0519*. In contrast, TnSeq of the *Msm* Δ*pbp-lipo* strain did not
406 reveal interactions with any other gene in the genome. The TnSeq data demonstrates that
407 despite being homologs, PBP-lipo in *Mab* and *Msm* are incorporated into different PG synthesis
408 networks. In *Mab,* this network renders PBP-lipo's function as essential for growth, whereas in
409 *Msm,* PBP-lipo is dispensable. Interestingly, in *Mtb* PBP-lipo became more required in a *ponA2*
410 knockout suggesting that PBP-lipo and PonA2 genetically interact *Mtb* (30) – a genetic
411 interaction that was not observed in *Mab*. This observation supports the hypothesis that PBP-
412 lipo is incorporated in different PG synthesis in *Mtb* as well.
413
414 In *Mab,* the three genes that genetically interacted with PBP-lipo, *pbpB, dacB1,* and *MAB_0519,*
415 are all hypothesized to be septal associated. PbpB is a D,D-transpeptidase that performs 4,3
416 crosslinking reactions at the septum. In both *E. coli* and *Msm*, depleting PbpB leads to cell
417 elongation and branching, reminiscent of the *Mab* PBP-lipo knockdown phenotypes (28). A
418 potential explanation of this genetic interaction is both PbpB and PBP-lipo perform 4,3-
419 crosslinking at the *Mab* septum. In this model, repressing both enzymes would dramatically
420 reduce 4,3-crosslinking at the septum and lead to cell death. It is possible that PBP-lipo and
421 PbpB have overlapping 4-3 cross-linking function at the septum. However, given that PBP-lipo
422 and PbpB are essential in *Mab*, both enzymes must have distinct functional roles. Their distinct
423 functions could be revealed by identifying unique genetic interactions each enzyme has with

424 other PG synthesis enzymes. Why *Mab* would require two PG 4,3 crosslinking enzymes
425 functioning at the septum is an intriguing area of future research.
426
427 The two other genes that synergized with PBP-lipo, DacB1 and MAB_0519, are both
428 hypothesized carboxypeptidases that cleave the terminal D-ala-D-ala on the pentapeptide
429 chains of PG monomers (42,43). This reaction is necessary for the subsequent 4,3 crosslinks
430 catalyzed by D-D transpeptidases like PbpB and PBP-lipo. Interestingly, DacB1 localizes to the
431 septum in *Mab* and has been described as septally localized in *Msm* and *Mtb* (44). Furthermore,
432 the homolog of MAB_0519 in *Mtb*, Rv3627c is involved in septal PG synthesis (45). Thus, we
433 hypothesize DacB1 and MAB_0519 are involved in septal PG synthesis and may work with
434 PBP-lipo to ensure proper septum formation. Interestingly, DacB1 and MAB_0519 are not
435 functionally redundant, given that both genes are synergistic with PBP-lipo. Further
436 characterization of the PG enzymes in *Mab* and their genetic networks will uncover species-
437 specific nuances in *Mab* PG synthesis that have the potential to be exploited for drug discovery.
438
439 Knockdown of PBP-lipo dramatically sensitized the reference *Mab* strain and 11 clinical isolates
440 to several antibiotics. The PBP-lipo knockdown was greater than 128-fold more sensitive to β-
441 lactams, ampicillin and amoxicillin, while other β-lactams like meropenem, cephalexin, ticarcillin
442 and others showed no difference in MIC. This result indicates a specific chemical-genetic
443 interaction between ampicillin/amoxicillin, and PBP-lipo. Historically, β-lactams have not been
444 used to treat *Mab* infections due to high levels of resistance and the presence of β-lactamases
445 (20). While imipenem and cefoxitin are used with some success, macrolides and
446 aminoglycosides remain the backbone of *Mab* treatment (46). Recently, studies have shown
447 dual β-lactam strategies are effective in killing *Mab* both *in vitro* and *in vivo* (47–49). These
448 synergy data suggest that understanding the specific antibiotic targets of β-lactams in *Mab*

449 would augment the design of effective dual β-lactam combinations. At the moment, effective
450 combinations are tested empirically with no insight into potential mechanisms (48). To address
451 this, Sayed *et al* used a combination of a bocillin FL binding assay to stain all the PBPs in *Mab*
452 followed by proteomics to identify the targets of 12 β-lactams and 2 β-lactamases. Interestingly,
453 in their datasets, PBP-lipo was not identified by mass spectrometry of bocillin FL-bounded PBPs
454 (50). This further supports our observation that PBP-lipo is expressed at low-levels in *Mab* and
455 is not identifiable by bocillin FL under native expression conditions.
456
457 Nonetheless, our data demonstrate that using a β-lactam or small molecules that target PBP-
458 lipo would not only kill the cell, but also potentiate β-lactams like ampicillin and amoxicillin. In
459 addition, the permeabilizing effect of PBP-lipo inhibition would potentiate drugs by allowing more
460 to enter the cell. Crucially, the observed synergy with PBP-lipo knockdown and β-lactams was
461 not just limited to the reference strain, but also present in 11 clinical isolates of *Mab,* indicating
462 that this synergy can be targeted for use in *Mab* clinical isolates.
463
464 Overall, this work employed TnSeq to identify the uniquely essential gene PBP-lipo in *Mab*. We
465 present PBP-lipo as a promising drug target given both its essentiality and its role in sensitizing
466 *Mab* to a range of antibiotics, including commonly used and accessible antibiotics, ampicillin
467 and amoxicillin. Future studies exploring the PBP networks of mycobacteria can expose further
468 species-specific vulnerabilities in peptidoglycan synthesis. Finally, identifying chemical inhibitors
469 of PBP-lipo may help form the foundation for new treatments against this emerging and difficult
470 to treat pathogen.

471 **Materials and Methods**
472

473 A full list of the strains, plasmids, and primers is available in Supplemental Tables 7, 8, and 9
474 respectively.

475
476 **Bacterial Strains and Culture Conditions:** All *M. abscessus (Mab)* and *M. tuberculosis (Mtb)*
477 strains were grown shaking at 37°C in liquid 7H9 media consisting of Middlebrook 7H9 salts
478 with 0.2% glycerol, 0.85 g/L NaCl, OADC (oleic acid, 5 g/L albumin, 2 g/L dextrose, 0.003 g/L
479 catalase), and 0.05% Tween80. *Mab* and *Mtb* were plated on Middlebrook 7H10 agar
480 supplemented with 0.5% glycerol. *M. smegmatis* mc2 155 *(Msm)* was grown shaking at 37°C in
481 liquid on 7H9 media consisting of Middlebrook 7H9 salts with 0.2% glycerol, 0.85 g/L NaCl,
482 ADC, and 0.05% Tween80 and plated on LB agar. Antibiotic selection concentrations for *Mab*
483 cultures were kanamycin 50 µg/µl and zeocin 100 µg/µl. For transposon mutant selection, 100
484 µg/ml of kanamycin was used. Antibiotic selection concentrations for *Msm* and *Mtb* cultures
485 were kanamycin 25 µg/µl, zeocin 20 µg/µl, and gentamicin 5 µg/µl. For *E. coli* (TOP10, XL1-
486 Blue and DH5α), all antibiotic concentrations were twice those of the concentrations used for
487 *Msm* and *Mtb*. Induction of all CRISPRi plasmids was performed with 500 ng/ul anhydrous
488 tetracycline (ATc).

489

490 **Strain Construction**

491 *Construction of 0, 1, 2, 3 sgRNA PBP-lipo knockdown strains and PBP-lipo complement strains*
492 To build the 0 sgRNA (empty sgRNA) *Mab* strain, we transformed the pCT296 vector containing
493 an empty sgRNA into *Mab.* To build the 1, 2, and 3 sgRNA strains, first we built individual
494 CRISPRi plasmids containing single sgRNAs that targeted PBP-lipo. These plasmids were cr25,
495 cr26, and cr56. We then designed primers that amplified the sgRNA targeting region with the
496 appropriate flanking sequences and performed Golden Gate cloning to combine the inserts into
497 one vector. This method was previously described by Rock et al (23). For the 1 sgRNA strain,

498 we transformed cr25 into the *Mab* strain. For the 2 sgRNA, we transformed the vector pCRC1,
499 which contained the cr25 and cr26 sgRNAs on one backbone. Finally, for the 3 sgRNA strain we
500 transformed pCRC2, which contained the cr25, cr26, and cr56 sgRNAs on one backbone.
501 To build the PBP-lipo complement strain, we designed primers to amplify PBP-lipo with modified
502 protospacer adjacent motif (PAM) sequences that were no longer homologous to the 1, 2, and 3
503 sgRNAs. This recoded PBP-lipo was then cloned into a constitutive expression vector resulting
504 in the pCA323 construct, which was transformed into the 2 sgRNA strain. The catalytically dead
505 mutant version of the recoded PBP-lipo was generated by using primers to generate the S364A
506 mutation. This engineered PBP-lipo was cloned into a constitutive expression vector and the
507 resulting construct, pCA324 was transformed into the 2 sgRNA strain.
508
509 *Msm* and *Mtb* ΔPBP-lipo strains
510 To generate PBP-lipo knockout mutants in *Msm* and *Mtb,* we used a recombineering approach
511 to replace the endogenous copy of the gene with a zeocin resistance cassette as previously
512 described (51). First, 500 base pairs of upstream and downstream sequence surrounding PBP-
513 lipo (*Rv2864c* and *MSMEG_2584c*) were amplified by PCR KOD XtremeTM Hot Start DNA
514 polymerase (EMD Millipore, Billerica, MA). These flanking regions were amplified with overlaps
515 for the zeocin resistance cassette. The 2 flanking regions and zeocin resistance cassette were
516 then assembled via isothermal assembly (52) into a single construct, which was then amplified
517 by PCR. Each deletion construct was transformed into either *Mtb* or *Msm* expressing inducible
518 copies of RecET for recombination (53). The resulting colonies were screened for PBP-lipo
519 deletion by PCR.
520
521 *PBP-lipo$_{Mab}$-strep expression strain*

522 PBP-lipo$_{Mab}$ was amplified using primers that added a C-terminal strep tag to the protein. The
523 resulting insert was Gibson stitched to the vector backbone that drove expression of PBP-
524 lipo$_{Mab}$-strep from the constitutively active MOP promoter.
525
526 *mRFP-PBP-lipo$_{Mab}$*
527 We amplified PBP-lipo$_{Mab}$ in two fragments. The first fragment contained the N-terminal signal
528 sequence of PBP-lipo. The second fragment contained the remainder of the protein. We then
529 amplified mRFP with overhangs that were compatible with the two halves of PBP-lipo. The
530 resulting three fragments were Gibson assembled to a vector backbone that constitutively drove
531 expression of the mRFP-PBP-lipo$_{Mab}$ fusion protein. A gly-gly-ser-gly-ser-gly linker was used in
532 between mRFP and the new N & C terminus of PBP-lipo.
533
534 *DacB1-GFPmut3*
535 DacB1 lacking a stop codon was amplified along with GFPmut3 containing overlaps with DacB1
536 and a gly-gly-ser linker. The two fragments were Gibson assembled to a vector backbone that
537 constitutively drove expression of the DacB1-GFPmut3 fusion protein.
538
539 **Growth Curve:** *Mab, Msm,* and *Mtb* cultures were grown to log phase and diluted to OD600
540 0.05. Growth curves were performed in a 96 well format at 37°C with shaking. OD600 was
541 measured every 15 min for 24-72 hr using the TECAN plate reader
542
543 **Colony Forming Units:** *Mab* and *Msm* cultures were grown to mid-log phase and then serially
544 diluted in their respective media in 96 well plates. Dilutions were then spot plated onto solid
545 media +/- 500 ng/ul ATc. Plates were incubated at 37°C for 4 days *(Mab)* or 3 days *(Msm)*. After
546 incubation, the resulting CFUs were calculated by counting the number of colonies at the
547 appropriate dilution. The fraction survivability was calculated as CFUs +ATc / -ATc.

548

549 **Minimum Inhibitory Concentration Determination:** *Mab, Msm,* and *Mtb* were grown to mid-
550 log phase and diluted to an OD600 = 0.003 in each well of non-treated 96-well plates (Genesee
551 Scientific) containing 100 µL of antibiotic serially diluted in 7H9 + OADC + 5 µg/mL clavulanate
552 (Sigma Aldrich). For MICs on *Mab* knockdown cells, cultures were induced for knockdown 18 hr
553 prior with 500 ng/ul ATc. Wells with knockdown bacteria also contained 500 ng/ul ATc. *Msm*
554 media contained ADC rather than OADC. Cells were incubated with drug at 37°C with shaking
555 for 1 day *(Mab, Msm)* or 7 days *(Mtb)*. Afterwards, 0.002% resazurin diluted in ddH_2O (Sigma
556 Aldrich) was added to each well. Plates were then incubated for 24 hr. MICs were determined
557 by the concentration of antibiotic that turned wells blue signifying no metabolic activity (54).
558

559 **Generation of Transposon Libraries:** To create transposon mutant libraries of *Mab* ATCC
560 19977 and *Msm* (wildtype and ΔPBP-lipo), 100 ml of bacterial cultures were grown to an OD600
561 of 1.5 – 2.0. For *Mab*, cultures were grown in biological triplicate. For *Msm*, the wildtype strain
562 was grown in duplicate while one replicate of the ΔPBP-lipo strain was grown. The cells were
563 then washed twice with 50 ml of MP Buffer (50mM Tris-HCl pH 7.5, 150 mM NaCl, 10 mM
564 $MgSO_4$, 2 mM $CaCl_2$) and resuspended in 1/10th the culture volume in MP Buffer. Afterwards, 2
565 x 10^{11} pfu of temperature sensitive φMycoMarT7 phage carrying the Himar1 transposon were
566 added to bacteria. Phage and bacterial cultures were incubated at 37°C for 4 hr with shaking.
567 The transduced cultures were spun down at RT 4000 rpm for 10 min and resuspended in 12 ml
568 of PBS-Tween. The cultures were then tittered by plating on 7H10 plates (*Mab)* or LB *(Msm)*
569 supplemented with kanamycin 100 µg/µml *(Mab)* or 20 µg/µl *(Msm)* before freezing the aliquots
570 for future plating. After determining the titer, 150,000 bacterial mutants of each transduced
571 culture were plated onto kanamycin selective plates and grown for 4 days at 37°C. The resulting
572 mutant libraries were harvested and stored in aliquots with 7H9 + 10% glycerol at -80°C.
573

574 **Genomic DNA Extraction:** To prep libraries for sequencing, we isolated the gDNA of the
575 mutant libraries using a bead-beating protocol developed in the lab. 2-6 ml of transposon mutant
576 libraries were thawed and spun down to remove excess glycerol in the sample. Pellets were
577 then resuspended in TE Buffer (10 mM Tris HCl pH 7.4, 1 mM EDTA pH8) and placed in bead-
578 beating tubes with 600 µl of phenol:chloroform. The samples were then bead-beat 4X for 45 s at
579 4000 rpm. Samples were cooled on ice for 45 s between each successive bead-beat round.
580 After bead-beating, the samples were spun down for 10 min at 13,000 rpm. The supernatant
581 was transferred to a new falcon tube and incubated with 1:1 volume phenol-chloroform for 1 hr
582 rocking. Samples were then spun down in MaXtract High Density phase-lock tubes (Qiagen) at
583 1500 g for 5 min. This separated the aqueous and organic layers. Afterwards, ½ volume of
584 chloroform was added to the tube and the contents were spun down at 1500 g for 5 min. The
585 aqueous phase was transferred to a new tube and RNAse A (Thermo Fisher) was added to a
586 final concentration of 25 µg/µl. The tubes were incubated at 37°C for 1 hr with shaking. Finally,
587 the supernatant was washed with 1:1 volume of phenol-chloroform followed by ½ volume of
588 chloroform. The aqueous phase was transferred to a new tube and genomic DNA was
589 precipitated with 1 volume of isopropanol alcohol and 1/10th volume of 3 M sodium acetate pH
590 5.2. The library gDNA was washed twice with fresh 70% ethanol and resuspended in nuclease
591 free ddH_2O. This protocol consistently generated high yields of *Mab* gDNA.
592
593 **Transposon sequencing, mapping, and analysis:** Sequencing libraries were prepared from
594 the extracted gDNA by amplifying chromosomal-transposon junctions following the protocol as
595 described by Long et al, 2015 (21). These amplicons were then sequenced using the Illumina
596 Hi-Seq platform. The resulting reads were mapped onto the *Mab* or *Msm* genomes. The data
597 were analyzed using the TRANSIT pipeline (22). Insertion counts at each TA site were
598 normalized using TTR normalization and averaged across replicates. Essentiality categories of
599 genes were determined by the Hidden Markov Model (HMM) algorithm in TRANSIT.

600 Resampling analysis was used to compare insertion accounts between genes in the wildtype
601 and ΔPBP-lipo *Msm* strains.
602
603 **Cloning of CRISPRi Constructs:** To clone sgRNAs onto the CRISPRi vector backbone,
604 complimentary targeting oligos were annealed and ligated (T4 DNA ligase, NEB) into the BsmBI
605 digested CRISPRi vector backbone. To clone multiple sgRNAs into the same vector, the
606 promoter, sgRNA handle, and sgRNA sequences were amplified with the appropriate flanking
607 sequences to perform Golden Gate cloning using the SapI cloning site in the CRISPRi vector
608 (23). All cloning was performed using DH5a cells and sequences were verified before
609 transformation into *Mab* and *Msm.*
610
611 **Transformation of *M. abscessus*:** To generate electrocompetent *Mab* cells, 50 ml of *Mab*
612 cultures were grown to mid-log phase. Cells were spun down at 4000 rpm for 10 min and
613 washed twice with pre-chilled 10% glycerol. Cell pellets were resuspended in 1/100th of the
614 starting volume and kept on ice for immediate use or stored at -80°C for future use. For
615 transformations ~100 ng of plasmid DNA was incubated with electro-competent cells for 5 min
616 before transforming the cells with 2500 V, 125 Ω, 25 μF. Afterwards, cells were recovered in 1
617 ml of 7H10 with OADC without selection for 3 hr at 37°C with shaking. Cells were then plated on
618 7H10 with the appropriate selection marker and incubated for 4 days at 37°C.
619
620 **Microscopy and Image Analysis:** All imaging was performed on an inverted Nikon TI-E
621 microscope at 60X and 100X magnification. For PBP-lipo knockdown experiments, cultures
622 were induced for knockdown with 500 ng/ul ATc for 18 hr prior to imaging. All *Mab* cultures were
623 fixed with 7H9 + 3% paraformaldehyde (PFA) for 1 hr and resuspended in PBS + 0.05%
624 Tween80 prior to imaging. Cellular features including cell length, width, and fluorescence signal

625 were analyzed using the OMEGA image analysis pipeline developed in the lab (Zhu et al,
626 unpublished).
627
628 **Fluorescent D-Amino Acid Staining:** NADA (3-[(7-Nitro-2,1,3-benzoxadiazol-4-yl)amino]-D-
629 alanine hydrochloride) was synthesized by Tocris following the published protocol (27). To stain
630 *Mab* with NADA, 0.1 mM of FDAA was added to 1 ml of exponentially growing cells and
631 incubated for 3 min before washing in warm 7H9 twice. For *Mab* imaging, after the second
632 wash, cells were fixed in 7H9 + 3% paraformaldehyde for 1 hr. The PFA was then washed off
633 and cells were resuspended in PBS + 0.05% Tween80 prior to imaging.
634
635 **RNA Extraction and RT-qPCR:** For each strain, cultures were grown in biological triplicate to
636 mid-log phase and then diluted back in +/- 500 ng/ml ATc and grown for 18 hr to achieve target
637 knockdown. Afterwards, 2 OD600 equivalents of cells from each culture were harvested by
638 centrifugation, resuspended in TRIzol (Thermo Fisher), and lysed by bead beating (Lysing
639 Matrix B, MP Biomedicals). Total RNA was extracted using the RNA miniprep (Zymo Research).
640 Residual genomic DNA was digested with TURBO DNase (Ambion), and samples were cleaned
641 with RNA clean-up columns (Zymo Research). cDNA was prepared using random hexamers
642 following manual instructions (Life Technologies Superscript IV). Alkaline hydrolysis was then
643 used to remove RNA. cDNA was purified by spin column (Qiagen) and then quantified by real-
644 time quantitative PCR (RT–qPCR) on a Viia7 light cycler (Applied Biosystems) using iTaq
645 Universal SYBR Green Supermix (BioRad). All qPCR primer pairs were confirmed to be >95%
646 efficient. The masses of cDNA used were experimentally validated to be within the linear
647 dynamic range of the assay. Signals were normalized to the *sigA* (*MAB_3009*) transcript and
648 quantified by the ΔΔCt method. Error bars are standard deviations from three biological
649 replicates.
650

651 **Bocillin FL staining:** *Mab* cultures were grown to mid-log phase and 10 OD units of bacteria
652 were spun down and resuspended in 1ml of fresh 7H9 media with 5 µg/ml of clavulanate.
653 Bocillin-BODIPY or FITC were added to cultures to a final concentration of 10 µM. Cells were
654 then incubated at 37°C for 2.5 hr, with aluminum wrapping to prevent light exposure. After
655 labeling, cells are washed with PBS + 0.05% Tween80 three times and resuspended in 200 µl
656 of lysis buffer (50 mM Tris-HCl pH = 7.4, 50 mM NaCl, protease inhibitor (Roche)). Samples
657 were bead beat 4X at 4000 rpm for 1 min with 1 min of rest on ice in between rounds of bead-
658 beats. $CaCl_2$ was added to a final concentration of 1 mM along with 4U of DNAse I and 10
659 mg/ml of fresh lysozyme. Samples were incubated at 37°C for 30 min. Afterwards, supernatants
660 were normalized by A280 protein concentration, diluted with 6X Laemmli buffer, and run on 4%–
661 12% NuPAGE Bis Tris precast gels (Life Technologies). To visualize fluorescence, we used a
662 BioRad Gel Doc system. To detect the presence of PBP-lipo-strep, we performed a Western
663 Blot. Membranes were blotted with rabbit α-Strep (GenScript) at 1:1000 in TBST + 3% BSA.
664
665 **Calcein Staining:** For each strain, cultures were grown in biological triplicate to mid-log phase
666 and diluted back in +/- 500 ng/ml ATc and grown for 18 hr to achieve target knockdown.
667 Afterwards, 3 OD units of bacteria were washed twice with PBS + 0.05% Tween80. Cells were
668 resuspended in PBS + 0.05% Tween80 and 100 µl of cells at OD600 = 0.4 was added to 96
669 well plates. The plates were incubated in the plate reader for 30 min at 37°C with shaking.
670 Afterwards, calcein was added at a final concentration of 1 µg/ml. Fluorescence signal was
671 measured every minute using the Tecan plate reader.
672

Acknowledgements

This project was funded by the generous support of the Paul and Daisy Soros Foundation, the NIH/NIAID F31 Predoctoral Fellowship award number F31AI149932, and award Number T32GM007753 from the National Institute of General Medical Sciences. The content is solely the responsibility of the authors and does not necessarily represent the official views of the National Institute of General Medical Sciences or the National Institutes of Health.

682 **References**

683 1. Bryant JM, Grogono DM, Rodriguez-Rincon D, Everall I, Brown KP, Moreno P, et al. Emergence and
684 spread of a human-transmissible multidrug-resistant nontuberculous mycobacterium. Science. 2016
685 Nov 11;354(6313):751–7.

686 2. Primm TP, Lucero CA, Falkinham JO. Health impacts of environmental mycobacteria. Clin Microbiol
687 Rev. 2004 Jan;17(1):98–106.

688 3. Johansen MD, Herrmann J-L, Kremer L. Non-tuberculous mycobacteria and the rise of
689 Mycobacterium abscessus. Nat Rev Microbiol. 2020 Feb 21;1–16.

690 4. Nessar R, Cambau E, Reyrat JM, Murray A, Gicquel B. Mycobacterium abscessus: a new antibiotic
691 nightmare. J Antimicrob Chemother. 2012 Apr;67(4):810–8.

692 5. Pang H, Li G, Wan L, Jiang Y, Liu H, Zhao X, et al. In vitro drug susceptibility of 40 international
693 reference rapidly growing mycobacteria to 20 antimicrobial agents. Int J Clin Exp Med.
694 2015;8(9):15423–31.

695 6. Jarand J, Levin A, Zhang L, Huitt G, Mitchell JD, Daley CL. Clinical and microbiologic outcomes in
696 patients receiving treatment for Mycobacterium abscessus pulmonary disease. Clin Infect Dis Off
697 Publ Infect Dis Soc Am. 2011 Mar 1;52(5):565–71.

698 7. Bryant JM, Brown KP, Burbaud S, Everall I, Belardinelli JM, Rodriguez-Rincon D, et al. Stepwise
699 pathogenic evolution of Mycobacterium abscessus. Science [Internet]. 2021 Apr 30 [cited 2021 Jun
700 18];372(6541).

701 8. van Opijnen T, Camilli A. Transposon insertion sequencing: a new tool for systems-level analysis of
702 microorganisms. Nat Rev Microbiol. 2013 Jul;11(7):435–42.

703 9. DeJesus MA, Gerrick ER, Xu W, Park SW, Long JE, Boutte CC, et al. Comprehensive Essentiality
704 Analysis of the Mycobacterium tuberculosis Genome via Saturating Transposon Mutagenesis. mBio
705 [Internet]. 2017 Mar 8 [cited 2020 Mar 28];8(1).

706 10. Foreman M, Gershoni M, Barkan D. A Simplified and Efficient Method for Himar-1 Transposon
707 Sequencing in Bacteria, Demonstrated by Creation and Analysis of a Saturated Transposon-Mutant
708 Library in Mycobacterium abscessus. mSystems [Internet]. 2020 Oct 27 [cited 2021 Mar 7];5(5).

709 11. Laencina L, Dubois V, Le Moigne V, Viljoen A, Majlessi L, Pritchard J, et al. Identification of genes
710 required for Mycobacterium abscessus growth in vivo with a prominent role of the ESX-4 locus.
711 Proc Natl Acad Sci U S A. 2018 30;115(5):E1002–11.

712 12. Rifat D, Chen L, Kreiswirth BN, Nuermberger EL. Genome-Wide Essentiality Analysis of
713 Mycobacterium abscessus by Saturated Transposon Mutagenesis and Deep Sequencing. mBio.
714 2021 Jun 15;e0104921.

715 13. Wong EB, Cohen KA, Bishai WR. Rising to the challenge: New therapies for tuberculosis. Vol. 21,
716 Trends in Microbiology. 2013. p. 493–501.

717 14. Bhat ZS, Rather MA, Maqbool M, Lah HU, Yousuf SK, Ahmad Z. Cell wall: A versatile fountain of
718 drug targets in Mycobacterium tuberculosis. Vol. 95, Biomedicine and Pharmacotherapy. 2017. p.
719 1520–34.

720 15. Jarlier V, Nikaido H. Mycobacterial cell wall: Structure and role in natural resistance to antibiotics.
721 FEMS Microbiol Lett. 1994 Oct 1;123(1–2):11–8.

722 16. Nasiri MJ, Haeili M, Ghazi M, Goudarzi H, Pormohammad A, Imani Fooladi AA, et al. New Insights in
723 to the Intrinsic and Acquired Drug Resistance Mechanisms in Mycobacteria. Front Microbiol. 2017
724 Apr 25;8:681.

725 17. Kieser KJ, Rubin EJ. How sisters grow apart: Mycobacterial growth and division. Vol. 12, Nature
726 Reviews Microbiology. Nature Publishing Group; 2014. p. 550–62.

727 18. Arora D, Chawla Y, Malakar B, Singh A, Nandicoori VK. The transpeptidase PbpA and noncanonical
728 transglycosylase RodA of Mycobacterium tuberculosis play important roles in regulating bacterial
729 cell lengths. J Biol Chem. 2018 Apr 27;293(17):6497–516.

730 19. Slayden RA, Belisle JT. Morphological features and signature gene response elicited by inactivation
731 of FtsI in Mycobacterium tuberculosis. J Antimicrob Chemother. 2009 Mar 1;63(3):451–7.

732 20. Soroka D, Dubée V, Soulier-Escrihuela O, Cuinet G, Hugonnet J-E, Gutmann L, et al.
733 Characterization of broad-spectrum Mycobacterium abscessus class A β-lactamase. J Antimicrob
734 Chemother. 2014 Mar;69(3):691–6.

735 21. Long JE, DeJesus M, Ward D, Baker RE, Ioerger T, Sassetti CM. Identifying essential genes in
736 Mycobacterium tuberculosis by global phenotypic profiling. Methods Mol Biol Clifton NJ.
737 2015;1279:79–95.

738 22. DeJesus MA, Ambadipudi C, Baker R, Sassetti C, Ioerger TR. TRANSIT--A Software Tool for Himar1
739 TnSeq Analysis. PLoS Comput Biol. 2015 Oct;11(10):e1004401.

740 23. Rock JM, Hopkins FF, Chavez A, Diallo M, Chase MR, Gerrick ER, et al. Programmable
741 transcriptional repression in mycobacteria using an orthogonal CRISPR interference platform. Nat
742 Microbiol. 2017 Feb 6;2(4):1–9.

743 24. Peters JM, Koo B-M, Patino R, Heussler GE, Hearne CC, Qu J, et al. Enabling genetic analysis of
744 diverse bacteria with Mobile-CRISPRi. Nat Microbiol. 2019 Feb;4(2):244–50.

745 25. Caro F, Place NM, Mekalanos JJ. Analysis of lipoprotein transport depletion in Vibrio cholerae using
746 CRISPRi. Proc Natl Acad Sci. 2019 Aug 20;116(34):17013–22.

747 26. Zhao G, Meier TI, Kahl SD, Gee KR, Blaszczak LC. BOCILLIN FL, a sensitive and commercially
748 available reagent for detection of penicillin-binding proteins. Antimicrob Agents Chemother. 1999
749 May;43(5):1124–8.

750 27. Kuru E, Tekkam S, Hall E, Brun YV, Van Nieuwenhze MS. Synthesis of fluorescent D-amino acids
751 and their use for probing peptidoglycan synthesis and bacterial growth in situ. Nat Protoc. 2015
752 Jan;10(1):33–52.

753 28. Wu KJ, Zhang J, Baranowski C, Leung V, Rego EH, Morita YS, et al. Characterization of Conserved
754 and Novel Septal Factors in Mycobacterium smegmatis. J Bacteriol. 2018 15;200(6).

755 29. Baranowski C, Welsh MA, Sham L-T, Eskandarian HA, Lim HC, Kieser KJ, et al. Maturing
756 Mycobacterium smegmatis peptidoglycan requires non-canonical crosslinks to maintain shape.
757 eLife. 2018 16;7.

758 30. Kieser KJ, Baranowski C, Chao MC, Long JE, Sassetti CM, Waldor MK, et al. Peptidoglycan
759 synthesis in Mycobacterium tuberculosis is organized into networks with varying drug susceptibility.
760 Proc Natl Acad Sci U S A. 2015 Oct 20;112(42):13087–92.

761 31. Slayden RA, Belisle JT. Morphological features and signature gene response elicited by inactivation
762 of FtsI in Mycobacterium tuberculosis. J Antimicrob Chemother. 2009 Mar;63(3):451–7.

763 32. Wissel MC, Weiss DS. Genetic Analysis of the Cell Division Protein FtsI (PBP3): Amino Acid
764 Substitutions That Impair Septal Localization of FtsI and Recruitment of FtsN. J Bacteriol. 2004
765 Jan;186(2):490–502.

766 33. Datta P, Dasgupta A, Singh AK, Mukherjee P, Kundu M, Basu J. Interaction between FtsW and
767 penicillin-binding protein 3 (PBP3) directs PBP3 to mid-cell, controls cell septation and mediates the
768 formation of a trimeric complex involving FtsZ, FtsW and PBP3 in mycobacteria. Mol Microbiol.
769 2006 Dec;62(6):1655–73.

770 34. Tortoli E, Kohl TA, Brown-Elliott BA, Trovato A, Leão SC, Garcia MJ, et al. Emended description of
771 Mycobacterium abscessus, Mycobacterium abscessus subsp. abscessus and
772 Mycobacteriumabscessus subsp. bolletii and designation of Mycobacteriumabscessus subsp.
773 massiliense comb. nov. Int J Syst Evol Microbiol. 2016 Nov;66(11):4471–9.

774 35. Allison F. Carey, Rock JM, Krieger IV, Chase MR, Fernandez-Suarez M, Gagneux S, et al. TnSeq of
775 Mycobacterium tuberculosis clinical isolates reveals strain-specific antibiotic liabilities. PLOS
776 Pathog. 2018 Mar 5;14(3):e1006939.

777 36. Medjahed H, Reyrat J-M. Construction of Mycobacterium abscessus defined glycopeptidolipid
778 mutants: comparison of genetic tools. Appl Environ Microbiol. 2009 Mar;75(5):1331–8.

779 37. Kieser KJ, Rubin EJ. How sisters grow apart: mycobacterial growth and division. Nat Rev Microbiol.
780 2014 Aug;12(8):550–62.

781 38. Datta P, Dasgupta A, Singh AK, Mukherjee P, Kundu M, Basu J. Interaction between FtsW and
782 penicillin-binding protein 3 (PBP3) directs PBP3 to mid-cell, controls cell septation and mediates the
783 formation of a trimeric complex involving FtsZ, FtsW and PBP3 in mycobacteria. Mol Microbiol.
784 2006 Dec;62(6):1655–73.

785 39. Rajagopalan M, Maloney E, Dziadek J, Poplawska M, Lofton H, Chauhan A, et al. Genetic evidence
786 that mycobacterial FtsZ and FtsW proteins interact, and colocalize to the division site in
787 Mycobacterium smegmatis. FEMS Microbiol Lett. 2005 Sep 1;250(1):9–17.

788 40. Datta P, Dasgupta A, Bhakta S, Basu J. Interaction between FtsZ and FtsW of Mycobacterium
789 tuberculosis *. J Biol Chem. 2002 Jul 12;277(28):24983–7.

790 41. Botella H, Yang G, Ouerfelli O, Ehrt S, Nathan CF, Vaubourgeix J. Distinct Spatiotemporal Dynamics
791 of Peptidoglycan Synthesis between Mycobacterium smegmatis and Mycobacterium tuberculosis.
792 mBio. 2017 12;8(5).

793 42. Ghosh AS, Chowdhury C, Nelson DE. Physiological functions of D-alanine carboxypeptidases in
794 Escherichia coli. Trends Microbiol. 2008 Jul 1;16(7):309–17.

795 43. Ealand CS, Asmal R, Mashigo L, Campbell L, Kana BD. Characterization of putative DD-
796 carboxypeptidase-encoding genes in Mycobacterium smegmatis. Sci Rep. 2019 Mar 26;9(1):5194.

797 44. Gorla P, Plocinska R, Sarva K, Satsangi AT, Pandeeti E, Donnelly R, et al. MtrA Response Regulator
798 Controls Cell Division and Cell Wall Metabolism and Affects Susceptibility of Mycobacteria to the
799 First Line Antituberculosis Drugs. Front Microbiol [Internet]. 2018 Nov 23 [cited 2020 May 27];9.

800 45. Zhang W, Li S, Ma L, Ding W, Xu Y. Identification of a novel carboxypeptidase encoded by Rv3627c
801 that plays a potential role in mycobacteria morphology and cell division. Enzyme Microb Technol.
802 2019 Jul 1;126:32–40.

803 46. Novosad SA, Beekmann SE, Polgreen PM, Mackey K, Winthrop KL. Treatment of Mycobacterium
804 abscessus Infection. Emerg Infect Dis. 2016 Mar;22(3):511–4.

805 47. Story-Roller E, Maggioncalda EC, Lamichhane G. Synergistic Efficacy of β-Lactam Combinations
806 against Mycobacterium abscessus Pulmonary Infection in Mice. Antimicrob Agents Chemother.
807 2019;63(8).

808 48. Pandey R, Chen L, Manca C, Jenkins S, Glaser L, Vinnard C, et al. Dual β-Lactam Combinations
809 Highly Active against Mycobacterium abscessus Complex In Vitro. mBio [Internet]. 2019 Feb 26
810 [cited 2020 May 9];10(1).

811 49. Lopeman RC, Harrison J, Rathbone DL, Desai M, Lambert PA, Cox JAG. Effect of Amoxicillin in
812 combination with Imipenem-Relebactam against Mycobacterium abscessus. Sci Rep. 2020 Jan
813 27;10(1):928.

814 50. Sayed ARM, Shah NR, Basso KB, Kamat M, Jiao Y, Moya B, et al. First Penicillin-Binding Protein
815 Occupancy Patterns for 15 β-Lactams and β-Lactamase Inhibitors in Mycobacterium abscessus.
816 Antimicrob Agents Chemother [Internet]. 2020 Dec 16 [cited 2021 Mar 24];65(1).

817 51. Boutte CC, Baer CE, Papavinasasundaram K, Liu W, Chase MR, Meniche X, et al. A cytoplasmic
818 peptidoglycan amidase homologue controls mycobacterial cell wall synthesis. Laub M, editor. eLife.
819 2016 Jun 15;5:e14590.

820 52. Gibson DG, Young L, Chuang R-Y, Venter JC, Hutchison CA, Smith HO. Enzymatic assembly of
821 DNA molecules up to several hundred kilobases. Nat Methods. 2009 May;6(5):343–5.

822 53. Murphy KC, Papavinasasundaram K, Sassetti CM. Mycobacterial recombineering. Methods Mol Biol
823 Clifton NJ. 2015;1285:177–99.

824 54. Kieser KJ, Boutte CC, Kester JC, Baer CE, Barczak AK, Meniche X, et al. Phosphorylation of the
825 Peptidoglycan Synthase PonA1 Governs the Rate of Polar Elongation in Mycobacteria. PLOS
826 Pathog. 2015 Jun 26;11(6):e1005010.

827
828

829

Figures and Legends

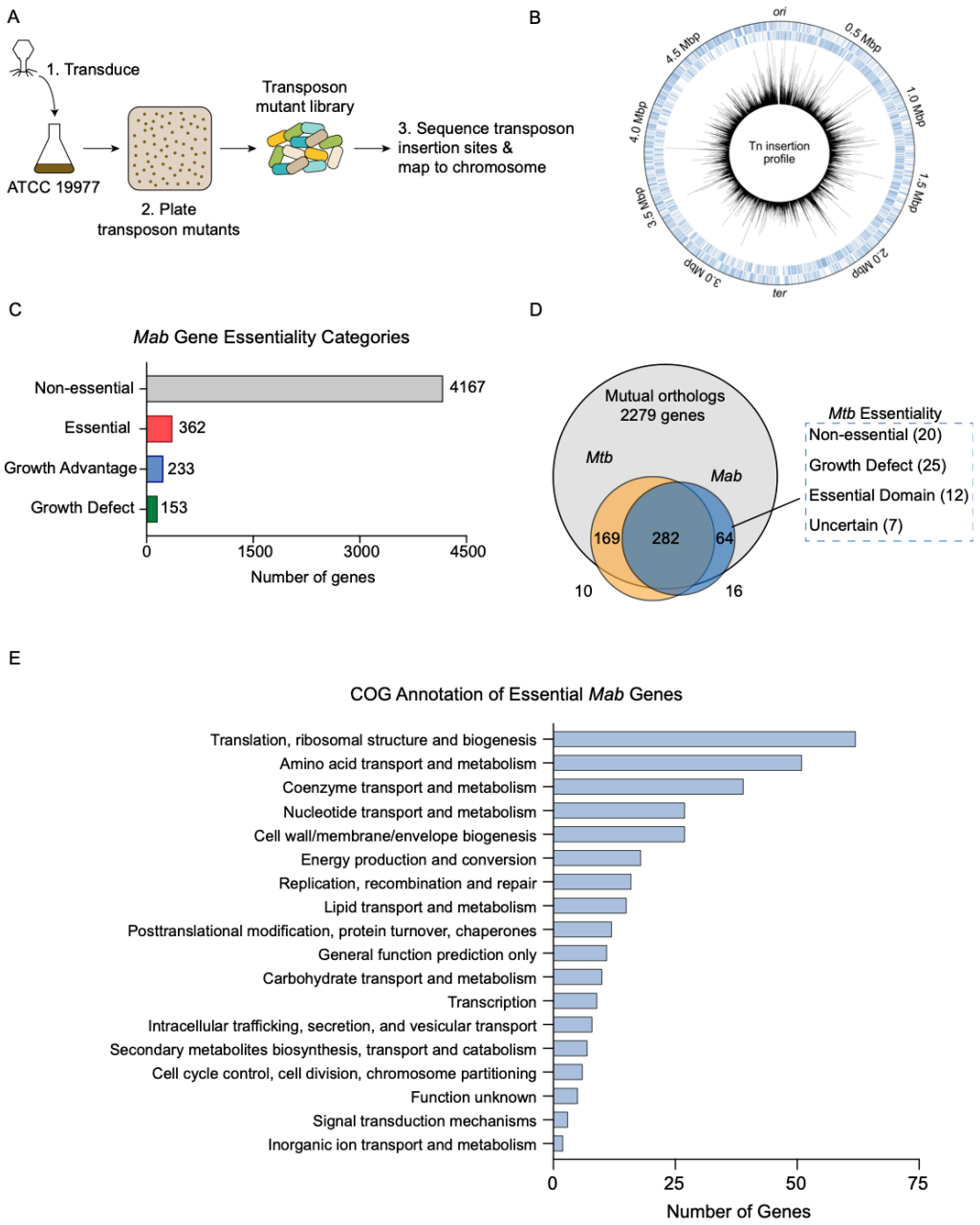

Figure 1. **Overview of TnSeq Analysis. (A)** Schematic of TnSeq protocol. Phage carrying Himar1 transposon is used to transduce *Mab* ATCC 19977 cultures. Over 51,000 independent transposon mutants were generated across three libraries **(B)** Location of transposon insertions in *M. abscessus subsp. abscessus* ATCC 19977 genome. Transposon insertions represent an average of the three replicates. Black bars represent number of insertions at each TA site. **(C)** Breakdown of gene essentiality categories. Essentiality calls were determined using the Hidden Markov Model (HMM) in TRANSIT **(D)** Essentiality comparison of mutual orthologs between *Mab* and *Mtb*. Venn Diagram shows 282 mutual orthologs are essential in both species. 20 essential *Mab* genes have mutual orthologs in *Mtb* that are non-essential. **(E)** COG (Clusters of Orthologous Group) categories of essential genes in *Mab*.

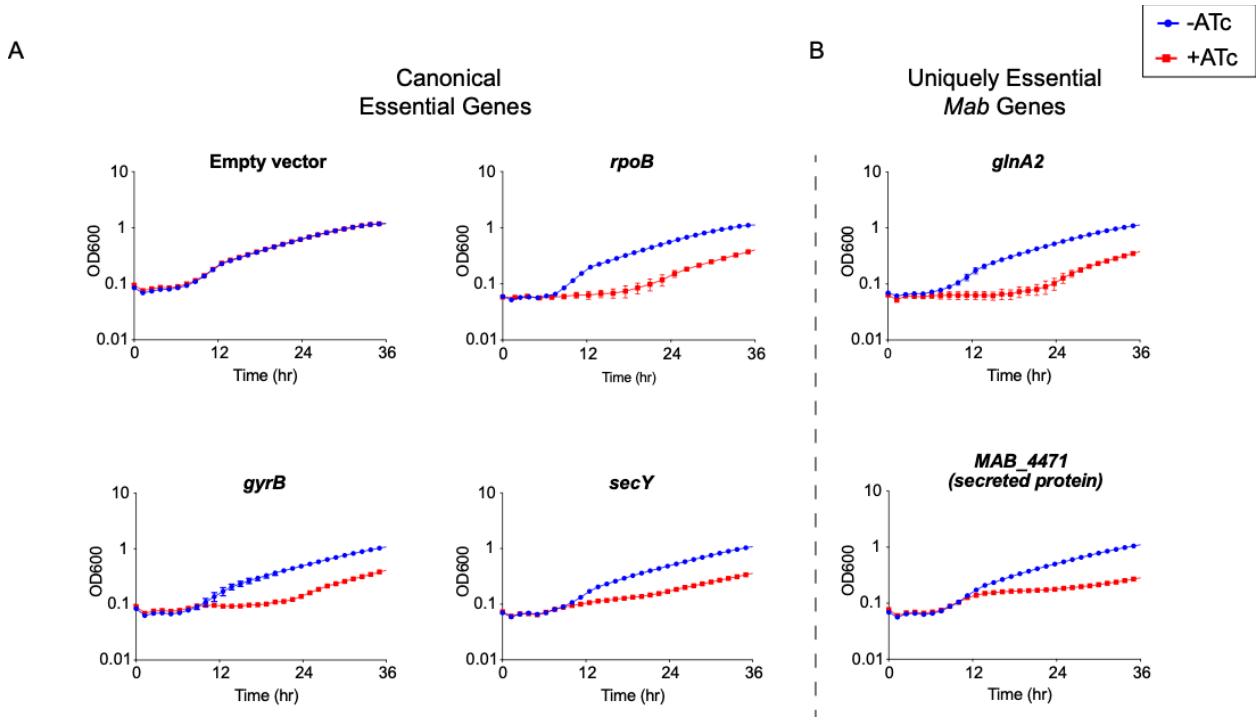

Figure 2. Validation of Essential Genes. (A) Growth curve of *Mab* strains with sgRNAs targeting canonical essential genes. **(B)** Growth curve of *Mab* strains with sgRNAs targeting uniquely essential *Mab* genes.

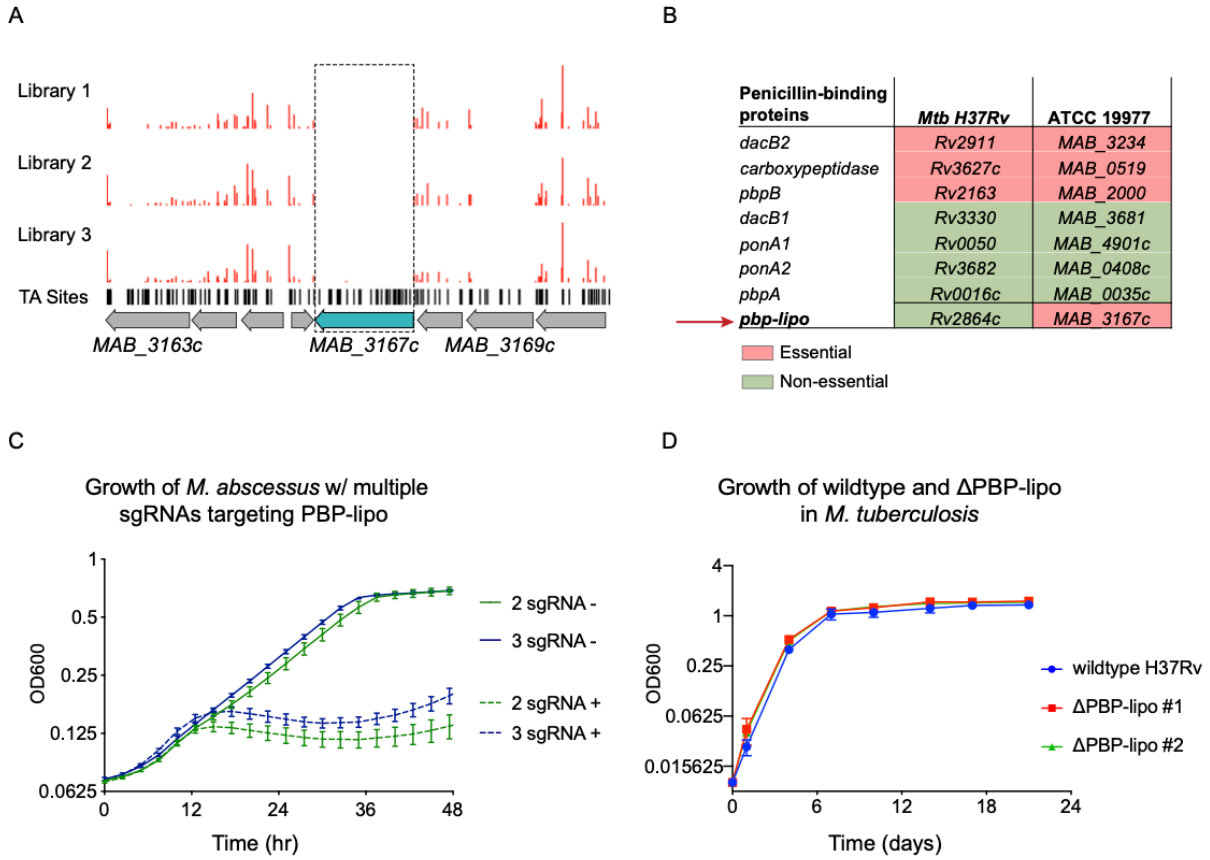

Figure 3. PBP-lipo is uniquely essential in *Mab* and non-essential in *Mtb*. (A) Transposon-insertion profile of PBP-lipo across three replicate transposon libraries. Red bars indicate the number of transposon insertions. Horizontal black lines indicate 'TA' sites, where the transposon inserts. Genes are schematized with gray arrows, with PBP-lipo colored in blue. Dotted box demarcates lack of insertions in PBP-lipo. **(B)** Comparison of essentiality for PBP orthologs between *Mtb* and *Msm*. **(C)** Growth of *Mab* cultures transformed with CRISPRi plasmid carrying either 2 or 3 sgRNAs targeting PBP-lipo. "-" symbol indicates cultures were grown without ATc. "+" symbol indicates cultures were grown with ATc. **(D)** Growth of wildtype *Mtb* and PBP-lipo knockout strains.

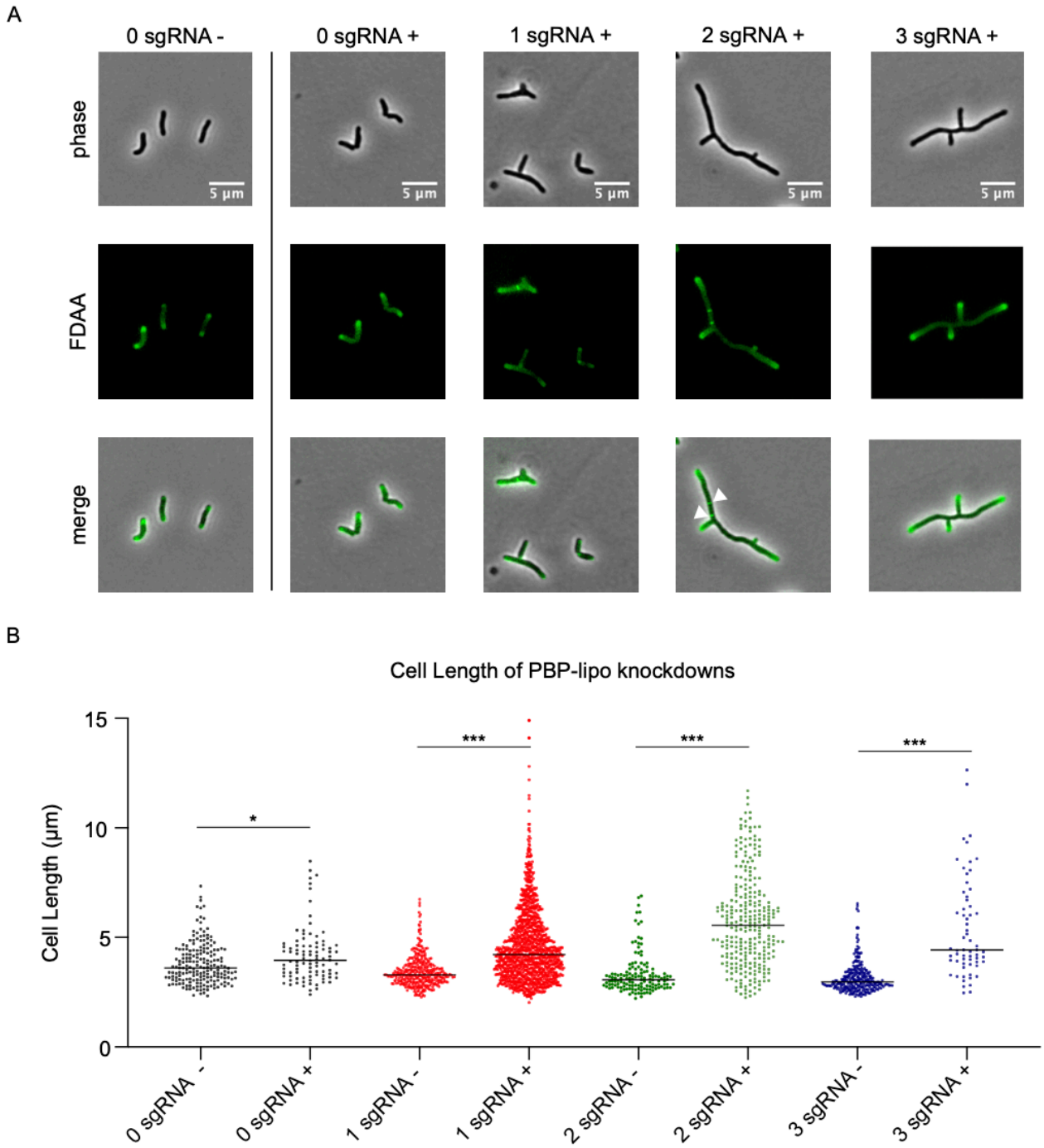

Figure 4. Knockdown of PBP-lipo disrupts cell morphology. **(A)** Microscopy images of PBP-lipo knockdown cultures. *Mab* strains carrying CRISPRi plasmids with either 0, 1, 2, or 3 sgRNAs targeting PBP-lipo. Arrows indicate sites of multiple septa formation. **(B)** Cell lengths of uninduced and induced strains. Measurements were obtained by image pipeline, OMEGA (Zhu *et al*, unpublished). Student's t test used to calculate the statistical difference in mean cell lengths. *** = p-val < 0.0001. * = p-val < 0.05.

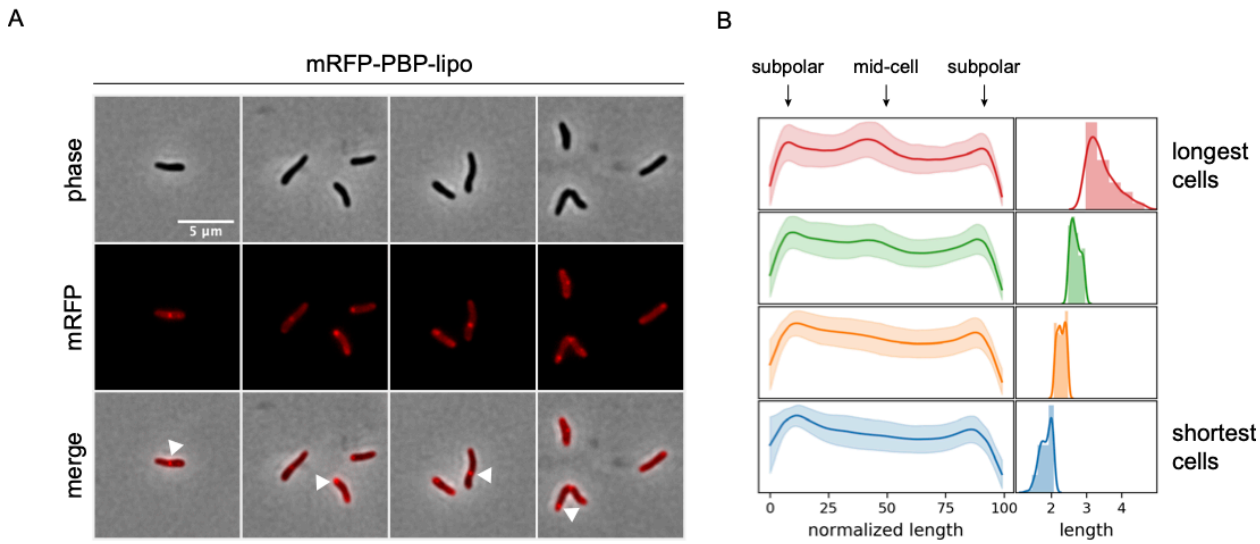

907
908
909 **Figure 5. PBP-lipo localizes to the subpolar region and the septum**. **(A)** Microscopy images of PBP-
910 lipo N-terminally tagged with mRFP. White arrows demarcate subpolar and septal localization of PBP-
911 lipo. **(B)** Quantification of mRFP signal along the length of the cell using OMEGA imaging pipeline (Zhu *et*
912 *al*, unpublished). Signal was normalized by cell length and cells were binned into quartiles based on
913 length.
914

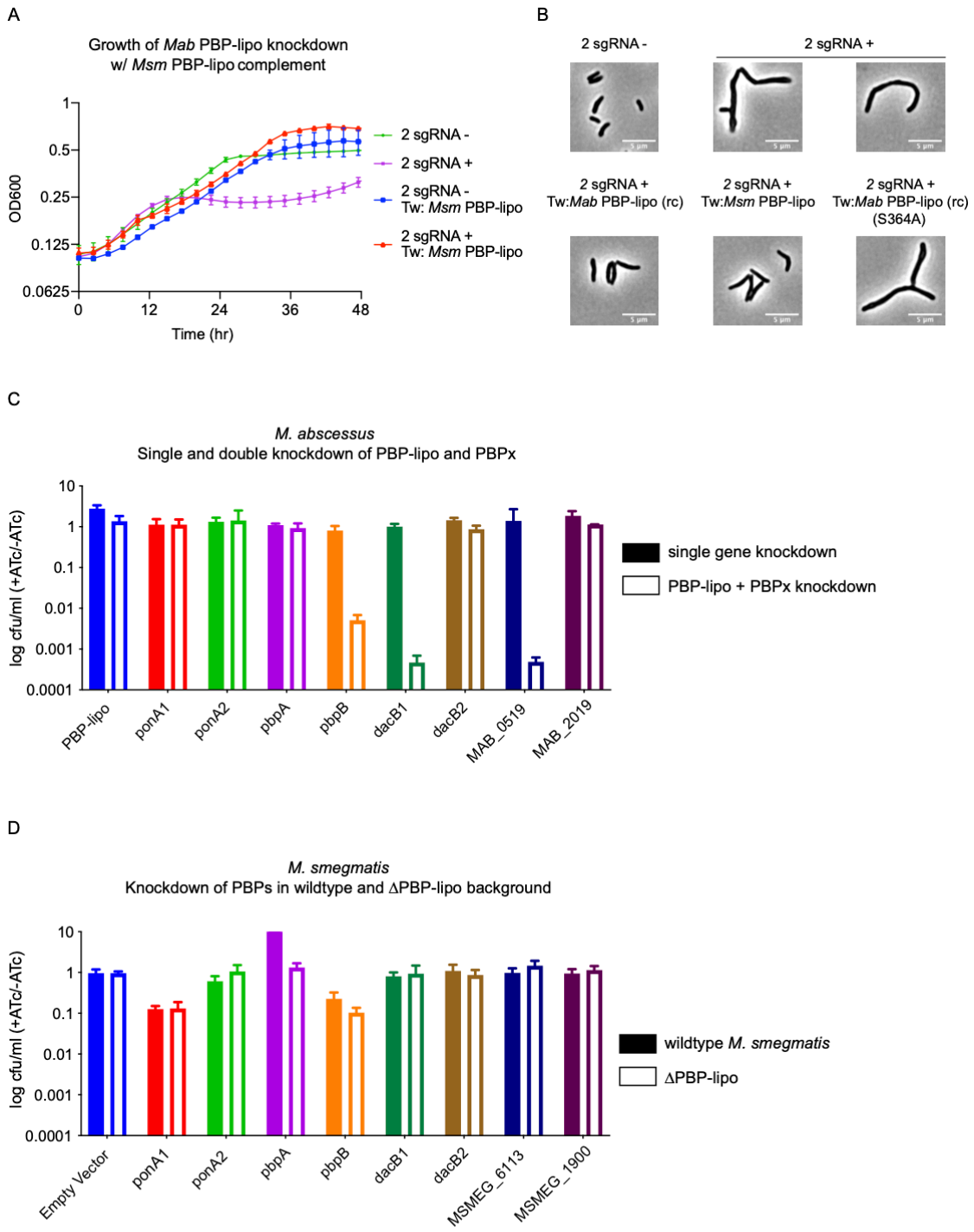

Figure 6. PBP-lipo network in *Mab* does not exist in *Msm*. (A) Growth curve of 2 sgRNA strain targeting PBP-lipo and 2 sgRNA strain with a constitutively expressed copy of PBP-lipo$_{Msm}$. **(B)** Microscopy images of 2 sgRNA and PBP-lipo complement strains. **(C)** Genetic synergy of PBP-lipo with other PBPs in *Mab*. Solid bar represents CFU of strains where a single PBP was knocked down. Open bar represents strains where PBP-lipo was knocked down in combination with the listed PBP. **(D)** Genetic synergy of PBPs and PBP-lipo in *Msm.* CRISPRi plasmids carrying sgRNAs targeting each of the PBPs in *Msm* were transformed into wildtype *Msm* (closed bar) and the ΔPBP-lipo mutant (open bar).

Table 1: Minimum Inhibitory Concentration (MIC) (µg/ml) of ATCC 19977 +/- PBP-lipo Knockdown

Antibiotic	-ATc	+ATc	Fold Difference
Cell Wall			
Ampicillin	>256	2	>128X
Amoxicillin	>256	2	>128X
Faropenem	8	1	8X
Cefoxitin	8	2	4X
Vancomycin	8	2	4X
Meropenem	128	128	N/A
Imipenem	>64	>64	“ “
Ticarcillin	>64	>64	“ “
Ceftazidime	>64	>64	“ “
Cephalexin	>64	>64	“ “
Ceftazidime	>64	>64	“ “
D-Cycloserine	>64	>64	“ “
Ethambutol	>64	>64	“ “
Isoniazid	>512	>512	“ “
Ribosome			
Clarithromycin	16	0.125	128X
Erythromycin	32	0.5	64X
Amikacin	16	4	4X
Clindamycin	>64	64	N/A
RNA Polymerase			
Rifampicin	32	2	16X
DNA Gyrase			
Ofloxacin	8	2	4X
Other			
Pyrazinamide	>64	>64	N/A
Pretomanid	>64	>64	“ “

925
926

927

Table 2: MIC (µg/ml) of *Mab* Clinical Isolates +/- PBP-lipo knockdown (Cell Wall Antibiotics)

	Ampicillin			Amoxicillin			Meropenem	
Clinical Isolate	**-ATc**	**+ATc**		**-ATc**	**+ATc**		**-ATc**	**+ATc**
ATCC 19977	>256	2		>256	2		128	128
T35	>256	< 0.5		>256	< 0.5		>256	256
T37	>256	< 0.5		>256	< 0.5		>256	256
T49	>256	4		>256	4		>256	128
T50	>256	4		>256	4		>256	128
T51	>256	2		>256	2		>256	256
T53	>256	4		>256	2		>256	256
T56	>256	<0.5		>256	<0.5		>256	128
BWH-B	>256	8		>256	2		>256	256
BWH-C	>256	4		>256	8		>256	256
BWH-E	>256	4		>256	2		>256	256

928
929

930

Table 3: MIC (µg/ml) of *Mab* Clinical Isolates +/- PBP-lipo Knockdown (Rifampicin and Clarithromycin)

	Rifampicin			Clarithromycin	
Clinical Isolate	**-ATc**	**+ATc**		**-ATc**	**+ATc**
ATCC 19977	32	2		16	0.125
T35	4	0.25		2	0.25
T37	16	1		2	0.25
T49	64	4		2	0.25
T50	32	1		16	0.25
T51	64	4		16	0.5
T53	32	1		8	0.5
T56	8	1		2	0.25
BWH-B	32	1		16	0.25
BWH-C	32	2		32	1
BWH-E	16	1		16	0.125

931